Evidence for Two Gaps and Breakdown of the Uemura Plot in $Ba_{0.6}K_{0.4}Fe_2As_2$ Single Crystals

Cong Ren*, Zhao-sheng Wang, Hui-qian Luo, Huan Yang, Lei Shan, and Hai-Hu Wen*
National Laboratory for Superconductivity, Institute of Physics and Beijing National Laboratory for Condensed Matter Physics, Chinese Academy of Sciences, P.O. Box 603, Beijing 100190, China

We report a detailed investigation on the lower critical field H_{c1} of the superconducting $Ba_{0.6}K_{0.4}Fe_2As_2$ (FeAs-122) single crystals. A pronounced kink is observed on the $H_{c1}(T)$ curve, which is attributed to the existence of two superconducting gaps. By fitting the data $H_{c1}(T)$ to the two-gap BCS model in full temperature region, a small gap of $\Delta_a(0) = 2.0 \pm 0.3$ meV and a large gap of $\Delta_b(0) = 8.9 \pm 0.4$ meV are obtained. The in-plane penetration depth $\lambda_{ab}(0)$ is estimated to be 105 nm corresponding to a rather large superfluid density, which points to the breakdown of the Uemura plot in FeAs-122 superconductors.

PACS numbers: 74.20.Rp, 74.25.Ha, 74.70.Dd

One of the crucial issues in understanding the superconducting mechanism in recently discovered FeAs-based layered superconductors [1, 2] is the pairing symmetry of the superconducting gap and the nature of the low energy excitations. For $LnFeAsO_{1-x}F_x$ (FeAs-1111) superconductors with $x = 0.04 \sim 0.2$ and Ln=La,Ce,Nd,Sm, reports on pairing symmetry are divided into two categories: those favoring a gap with [3, 4, 5, 6, 7] or without [8, 9, 10] nodes. In other aspect, the upper critical field measurement [11], tunneling spectroscopy [12], NMR [13], magnetic penetration depth measurement [14, 15] and Mössbauer [16] experiments indicate the existence of a two-gap nature. However, because most of the current experiments were performed on polycrystalline samples, the experimental results within the context of pairing symmetry have not yet reached a consensus.

The emergence of $(Ba,Sr)_{1-x}K_xFe_2As_2$ (FeAs-122) [17, 18] hole-doped superconductors with transition temperature T_c up to 38 K has enriched the research in this area. Although stoichiometric (undoped) $BaFe_2As_2$ shares the same feature with undoped LnFeAsO of a spin density wave type magnetic order and a structural transition at similar temperatures [19, 20], however, there are also some significant differences between the properties of FeAs-1111 and FeAs-122 superconductors. Most notable is the fact that FeAs-1111 superconductors seem to have very low charge carriers density [2] and hence low superfluid density [5, 21]. This may give explanation to the fact that the Uemura plot is satisfied in the FeAs-1111 systems [21, 22]. According to Uemura *et.al.* [23], in superconductors with low superfluid density (ρ_s), T_c scales linearly with $\rho_s \propto \lambda_{ab}^{-2}(0)$, this is actually not required by the BCS theory. However, it is found that the charge carrier density in FeAs-122 is an order of magnitude larger than those in FeAs-1111 systems [17, 24]. Thus it is very interesting to know whether the Uemura plot is still satisfied in FeAs-122 superconductors.

Lower critical field $H_{c1}(T)$, or equivalently, magnetic penetration depth $\lambda(T)$ are fundamental probes of the nature of the pairing symmetry, or/and multigap of unconventional superconductors. As an advantage, $H_{c1}(T)$ measurement probes relatively large depths (in scale of $\lambda \sim 100$ nm) and are insensitive to sample surface condition. In this Letter we present the first detailed magnetic penetration measurements of superconducting $Ba_{0.6}K_{0.4}Fe_2As_2$ single crystals. The local magnetization measurements allow a precise determination of H_{c1}. We found the presence of possibly a full gap feature together with two gaps in $Ba_{0.6}K_{0.4}Fe_2As_2$ superconductors. Meanwhile, the absolute value of $H_{c1}(0)$ determined from this work place the samples far away from the Uemura plot.

Crystals of $Ba_{0.6}K_{0.4}Fe_2As_2$ were grown by FeAs flux method. The details of crystal synthesis have been described elsewhere [24]. Our crystals were characterized by both resistivity and ac susceptibility measurements with $T_c = 36.2$ K and a transition width of $\Delta T_c = 0.45$ K (10%-90% of normal state resistivity) [24], as displayed in left inset of Fig.1 (a). A single crystal (sample No. 1) was selected from the cleaved as-grown bulk under optical microscope. The sample has dimensions of 110 μm in diameter and 40 μm in thickness, as shown in the right inset of Fig. 1(a). The crystal structure was examined by X-ray Diffraction (XRD), and a typical diffraction pattern was shown in the main panel of Fig. 1(a). Only $(00l)$ peaks were observed with the full-width-at-half-maximum (FWHM) around 0.1 °, which indicates good crystallization of our samples.

The local magnetization measurement was performed on two crystals using a two dimensional electron gas (2DEG)-based micro Hall sensor with an active area of 10×10 μm^2. The Hall sensor was characterized without sample attachment at different temperatures, the Hall coefficient R_H was identical to 0.22 Ω/Oe, independent of T below 80 K. In our experiment, we used a small field sweep rate of 30 Oe/min to measure the isothermal magnetization $M(H)$ curves in both decreasing (M_{dec}) and increasing (M_{inc}) the fields to minimize the complex effects of the character of the field penetration in a layered

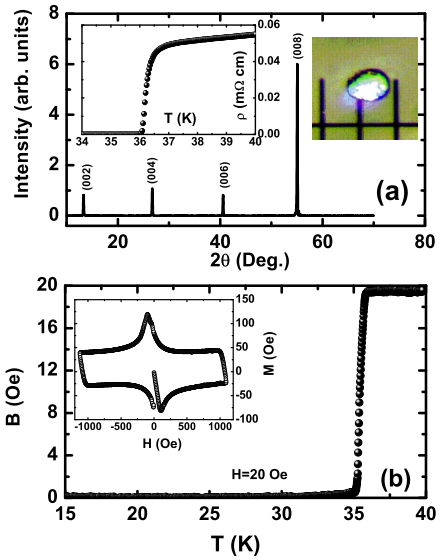

FIG. 1: (Color online) (a) X-ray diffraction pattern of the $Ba_{0.6}K_{0.4}Fe_2As_2$ crystal. The right inset shows the sample (No. 1) under the optical microscope. The scale underneath with 100 μm/grid is used to display the size of the sample. The left inset shows the resistive transition on one crystal cut from the same piece as the one for the measurement of H_{c1}. (b) The induction B by Hall probe as a function of T measured in zero-field-cooled mode with applied field. Inset: A typical magnetization hysteresis loop measured at 32.1 K by the Hall sensor.

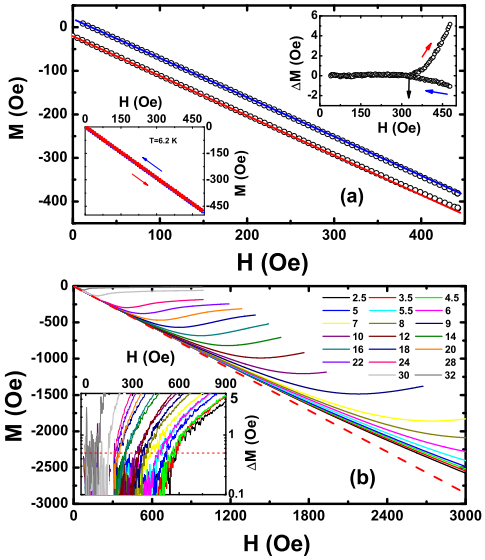

FIG. 2: (Color online) (a) A typical magnetization hysteresis loop (symbols), the solid lines are the linear fitting curves using the low field data (Meissner line). The increasing and decreasing branches are shifted downward and upward, respectively for clarity. The same case is shown in the bottom-left inset when the maximum field is less than H_{c1}. The upper-right inset shows the magnetization data subtracted the Meissner line. The arrows indicate the direction of sweeping fields and the determination of H_{c1}. (b) The initial part of the magnetization curves $M(H)$ of sample No. 2 at various temperatures. The dashed line gives the Meissner linear approach. Inset: The same magnetization data in field subtracted by the Meissner line. The dashed line in the inset sets up a criterion of 0.5 Oe.

structure [25]. A second crystal (sample No. 2) with dimensions of $210\times150\times50$ μm^3 was also measured by Hall sensor and vibrating sample magnetometry (VSM), and both measurements showed essentially identical behavior except for the different demagnetization effect.

In order to check whether the vortex entry is influenced by the Bean-Levingston surface barrier[26, 27], we measured the magnetization hysteresis loops. The result is shown in the inset of Fig. 1(b). The $M(H)$ curve shows a symmetric feature at $T = 32.1$ K which is close to T_c, indicative of the dominance of bulk pinning and the absence of the Bean-Levingston surface barrier for vortex entry.

The quality of the crystal and the accuracy of the local magnetization measurement were demonstrated in Fig. 1(b), in which the induction $B = H + 4\pi M$ sensed by the Hall probe is plotted as a function of T under a bias field $H = 20$ Oe. The superconducting transition can be detected as the induction jump at $T_c = 35.8$ K with a width of $\Delta T_c = 0.5$ K, which shows the high quality of the crystal. As shown in raw data of $B(T)$, at low temperatures, B is close to 0, implying a full Meissner shielding effect: $4\pi M \simeq -H$. Alternatively, the magnitude of the change in B measured by the Hall sensor through the superconducting transition is 19.8 Oe, very close to the applied magnetic field 20 Oe. Thus the achievement of full Meissner shielding effect in our measurement provides a reliable way to determine the value of H_{c1}.

Shown in Fig.2(a) are the typical isothermal $M(H)$ curves by taking M_{dec} and M_{inc} at T=17.1 K, respectively. It can be seen that, at low H, the M_{dec} and M_{inc} are fully reversible, showing a common linear dependence of the magnetization on field as displayed in the bottom-left inset of Fig. 2(a). At high H, a deviation from the linear dependence occurs at $H = H_{c1}$ for both M_{dec} and M_{inc} curves. To distinguish these deviations, we fit more than 50 data points between 10 and 30 Oe by a linear relation to account for the common linear dependence of $M(H)$. These fitted linear lines describe the Meissner shielding effects ("Meissner line") at low fields, as evidenced quantitatively in Fig. 2(a) in which the slope of the fitted lines are -0.98, being very close to -1. Thus the deviation of $M(H)$ from the linear Meissner shielding is an indication of the first penetration field H_{c1}. An alternative way to determine the value of H_{c1} from these reversible isothermal $M(H)$ curves is to subtract the Meissner line from both $M_{dec}(H)$ and $M_{inc}(H)$ curves, as illustrated in the upper-right inset of Fig. 2(a).

The threshold field of non-zero magnetization happens to be the divergence of the increasing and decreasing $M(H)$ curves. It is noted that the values of H_{c1} with this criterion were determined in both increasing and decreasing field, so they are the true thermodynamic values and are not altered by the surface barrier [25].

For a strict treatment, we determined the value of H_{c1} by examining the point of departure from the Meissner line on the initial slope of the $M(H)$ curve. In the inset of Fig. 2(b) we show how to determine H_{c1} by using a criterion of $B = \Delta M = 0.5$ Oe at different temperatures. For a quantum flux $\phi_0 = 20.7$ Oe μm^2, $\Delta M = 0.5$ Oe is equivalent to about $(2 \sim 3)\phi_0$ penetrating into the (10×10) μm^2 sensing area, which is the limit of our Hall probe technique. The H_{c1} values determined in this way are about 4% larger than those estimated from the point where the reversible magnetization deviates from linearity, and we did not observe any significant difference in the T-dependence of H_{c1} deduced from either of the two criterion.

Shown in Fig. 3(a) and (b) are the main results of our experiment, in which the obtained H_{c1} are plotted as a function of T for crystals No. 1 and 2, respectively. At $T < 4 \sim 5$ K, $H_{c1}(T)$ is weakly T-dependent and seems to show a tendency towards saturation at lower T (in the limited temperature range). As illustrated in the insets of Fig. 3(a) and (b), the saturated H_{c1} reach 695 Oe for sample No. 1 and 590 Oe for sample No. 2. This tendency of $H_{c1}(T)$ reflects a possible fully gapped nature of superconducting state at low T for $Ba_{0.6}K_{0.4}Fe_2As_2$ superconductors, although we could not rule out the possibility of a small gap with nodes in the dirty limit.

A pronounced *kink* can be easily observed in $H_{c1}(T)$ curves at $T \sim 15$ K for both samples. Obviously, the occurrence of the kink in $H_{c1}(T)$ can not be explained by the model with an s-wave or d-wave *single gap*. On the other hand, this kinky structure in $H_{c1}(T)$ resembles that of the related penetration depth of the two-band superconductor MgB_2 [28], in which a positive curvature was observed and explained by the multi-band theory [29]. In addition, recent ARPES measurement resolved a two-gap nature in a similar $Ba_{0.6}K_{0.4}Fe_2As_2$ crystal [30, 31]. Thus our observation of a kink in $H_{c1}(T)$ strongly suggests the existence of multiple gaps in $Ba_{0.6}K_{0.4}Fe_2As_2$ superconductors, being consistent with that predicted in electronic band structure calculations [32].

Quantitatively we analyze and discuss in more detail the data of $H_{c1}(T)$ to elucidate the related gap function. For our crystals, assuming $\lambda_{ab}(0) \sim 100 - 200$ nm [33], the coherence length $\xi_{ab}(0)$ was estimated to be 2-2.5 nm from an extremely high upper critical field H_{c2} $[\mu_0 H_{c2}^{//c}(0) = \phi_0/2\pi\xi_{ab}^2(0)]$ [24, 34], and the mean free path (determined from the resistivity at 38 K) is ~ 15 nm, our samples are therefore expected to be in the moderately clean, local limit. In this case the local London model is valid to describe the data. For a single gap superconductor, H_{c1} relates the normalized superfluid density as: $\widetilde{\rho}_s(T) \equiv \lambda_{ab}^2(0)/\lambda_{ab}^2(T) = H_{c1}(T)/H_{c1}(0)$, and $\widetilde{\rho}_s(T)$ is given by [35, 36]

$$\widetilde{\rho}_s(T) = 1 + 2\int_0^\infty \frac{\mathrm{d}f(E)}{\mathrm{d}E}\frac{E}{\sqrt{E^2 - \Delta(T)^2}}\mathrm{d}E \qquad (1)$$

with f the Fermi function. Here the total energy is $E = \sqrt{\epsilon^2 + \Delta^2}$, and ϵ is the single-particle energy measured from the Fermi surface. It is assumed that the gap Δ on each Fermi surface follows the weak-coupling BCS temperature dependence. For a superconductor with two gaps, the normalized superfluid density may be written as

$$\widetilde{\rho}_s = x\widetilde{\rho}_s{}^a + (1-x)\widetilde{\rho}_s{}^b, \qquad (2)$$

where x is the fraction of superfluid density $\widetilde{\rho}_s{}^a$ associated with the small gap Δ_a. The results of the calculations and H_{c1} of sample No. 1 and 2 are shown by the red solid lines in Fig. 3(a) and (b), respectively. Fitting the data to above equations (with two s-wave gaps) yields: $\Delta_a = 1.6 \pm 0.3$ meV, $\Delta_b = 9.1 \pm 0.3$ meV and x=0.72 for sample No.1, and $\Delta_a = 2.2 \pm 0.2$ meV, $\Delta_b = 8.8 \pm 0.3$ meV and x=0.70 for sample No.2. The gaps obtained from our $H_{c1}(T)$ measurements are clearly smaller than those determined from the ARPES measurements[30, 31]. This

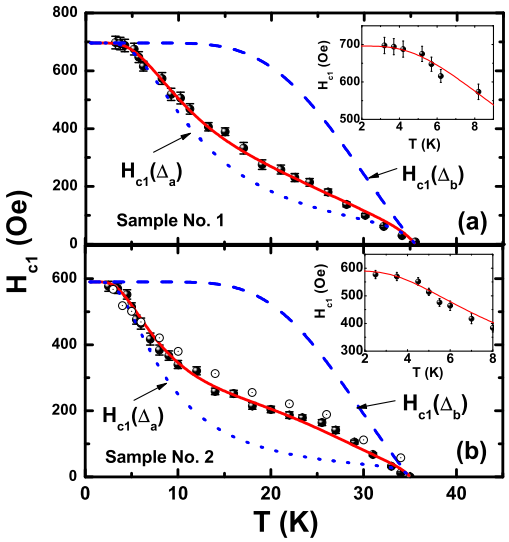

FIG. 3: (Color online) The extracted H_{c1} as a function of T for sample No.1 (a) and No.2 (b)(full circles with error bars). The open dotted circles in (b) represent the H_{c1} determined from the VSM measurements taken into account of the demagnetization effect. The solid lines are the fitting curves using the two-gap model [Eq.(1) and Eq.(2)]. The contributions of the small gap $[H_{c1}(\Delta_a)]$ and the large gap $[H_{c1}(\Delta_b)]$ in the model are also shown by the dotted and dashed lines, respectively. The two insets in (a) and (b) show the enlarged views of the data $H_{c1}(T)$ in low temperature region together with the theoretical fitting curves (solid lines) with a two-gap model.

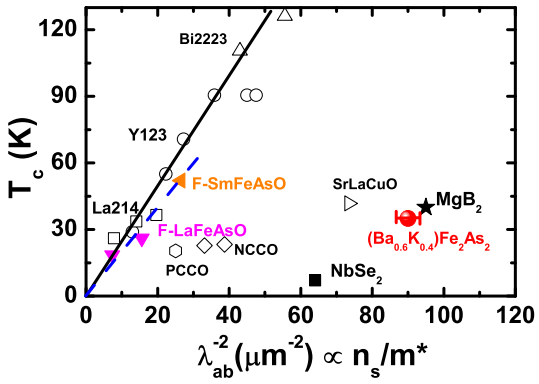

FIG. 4: (Color online) The correlations between T_c and the superfluid density n_s/m^*. Points for the cuprates are taken from Ref.21,22. The full triangles are showing the data for F-LaFeAsO (Ref.5 and Ref.21) and F-SmFeAsO (Ref.13 and our work), both are close to the Uemura plot of the cuprate superconductors. The data of the FeAs-122 phase (the red full circle), MgB_2 and $NbSe_2$ are far away from the general Uemura plot [23].

discrepancy may be induced by the different ways and different criterions in determining the gaps, this should be checked by future experiments. It is interesting to note that the large gap accounts for only 30% of the total superfluid density. We must stress that although a small gap with nodes (in the dirty limit) cannot be excluded from our low temperature data, this will not lead to a significant change to the general fitting results obtained here.

Another important result of our experiment, the absolute value of $\lambda_{ab}(0)$ is *independently* deduced from the measured $H_{c1}(0)$. In principle, we evaluate the penetration depth $\lambda_{ab}(0)$ using the expression: $H_{c1}^{//c} = (\phi_0/4\pi\lambda_{ab}^2)\ln\kappa$, where $\kappa = \lambda/\xi$ is the Ginzburg-Landau parameter (here we assume that κ is T-independent). Using $H_{c1}^{//c}(0) = 695$ Oe and $\kappa = 80$, we obtain $\lambda_{ab}(0) \simeq 105$ nm for sample No. 1 and 115 nm for sample No. 2. The value of $\lambda_{ab}^{-2}(0)$, or equivalently the condensed carrier density n_s/m^* (superconducting carrier density/effective mass), allows us to check whether the well-known scaling behaviors between n_s/m^* and T_c still works for the present system. In Fig. 4 we present our results together with many others, including the FeAs-1111 system, cuprates, MgB_2 and $NbSe_2$ [37]. It is remarkable that $Ba_{0.6}K_{0.4}Fe_2As_2$ resides far away from the Uemura plot, which is contrasted by the case of the FeAs-1111 system which is quite close to the Uemura plot. This discrepancy between FeAs-122 and FeAs-1111 implies very essential difference between the physics in the two systems, this warrants further investigations.

To summarize, we conduct magnetization measurements on $Ba_{0.6}K_{0.4}Fe_2As_2$ single crystals, and the lower critical field $H_{c1}(T)$ is reliably extracted. It is found that H_{c1} exhibits a pronounced kink at $T \sim 15$ K, which indicates a multi-gap nature. By using the two-gap weak coupling BCS model to fit the data, we obtained a small gap of $\Delta_a(0) \simeq 2.0 \pm 0.3$ meV and a large gap of $\Delta_b(0) \simeq 8.9 \pm 0.4$ meV. An estimate of the in-plane penetration depth gives $\lambda_{ab}(0) \simeq 105$ nm, which points to the breakdown of the Uemura relation for the optimally doped $Ba_{0.6}K_{0.4}Fe_2As_2$ superconductors.

Acknowledgement: The authors are grateful to Junren Shi, Tao Xiang and Jan Zaanan for helpful discussions, and Wen-Xin Wang and Hong Chen for providing us the GaAs/AlGaAs substrates. This work is supported by the Natural Science Foundation of China, the Ministry of Science and Technology of China (973 project No: 2006CB60100, 2006CB921107, 2006CB921802), and Chinese Academy of Sciences (Project ITSNEM).

* cong_ren@aphy.iphy.ac.cn
* hhwen@aphy.iphy.ac.cn

[1] Y. Kamihara *et al.*, *J. Am. Chem. Soc.* **130**, 3296 (2008).
[2] G. F. Chen *et al.*, *Phys. Rev. Lett.* **100**, 247002 (2008); Xiyu Zhu *et al.*, *Supercond. Sci. Technol.* **21**, 105001 (2008); X. H. Chen *et al.*, *Nature* **453**, 761 (2008); Z. A. Ren *et al.*, *Chin. Phys. Lett.* **25**, 2215(2008).
[3] Gang Mu *et al.*, *Chin. Phys. Lett.* **25**, 2221 (2008).
[4] Lei Shan *et al.*, to be published on *EuroPhys. Lett.*.
[5] Cong Ren *et al.*, arXiv:0803.0928.
[6] Yusuke Nakai *et al.*, arXiv:0804.4765.
[7] M.C. Boyer *et al.*, arXiv:0806.4400.
[8] T. Y. Chen *et al.*, *Nature* **453**, 1224 (2008).
[9] K. Hashimoto *et al.*, arXiv:0806.3149.
[10] C. Martin *et al.*, arXiv:0807.0807.
[11] F. Hunte *et al.*, *Nature* **453**, 903 (2008).
[12] Y. L. Wang *et al.*, arXiv:0806.1986,
[13] K. Matano *et al.*, *EuroPhys. Lett.* **83**, 57001 (2008).
[14] L. Malone *et al.*, arXiv:0806.3908.
[15] S. Wyeneth et al., arXiv:0806.1024.
[16] Israel Felner *et al.*, arXiv:0805.2794.
[17] M. Rotter, M. Tegel, D. Johrendt, arXiv:0805.4630.
[18] K. Sasmal *et al.*, arXiv:0806.1301.
[19] M. Rotter *et al.*, arXiv:0805.4021.
[20] Q. Huang, *et al.*, arXiv:0806.2776.
[21] H. Luetkens *et al.*, arXiv:0804.3115.
[22] J. P. Carlo *et al.*, arXiv:0805.2186.
[23] Y. J. Uemura *et al.*, *Phys. Rev. Lett.* **66**, 2665 (1991)
[24] H. Q. Luo *et al.*, arXiv:0807.0759.
[25] Ruixing Liang *et al.*, *Phy. Rev. Lett.* **94**, 117001 (2005).
[26] E. Zeldov *et al.*, *Phys. Rev. Lett.***73**, 1428(1994).
[27] M. Konczykowski, L. I. Burlachkov, Y. Yeshurun, F. Holtzberg, *Phys. Rev. B* 43, 13707 (1991).
[28] F. Manzano *et al.*, *Phys. Rev. Lett.***88**, 047002 (2002).
[29] A. A. Golubov *et al.*, *Phys. Rev. B* **66**, 054524 (2002).
[30] H. Ding *et al.*, *EuroPhys. Lett.* **83**, 47001 (2008).
[31] L. Zhao *et al.*, arXiv:0807.0398.
[32] F. Wang, arXiv:0807.0498.
[33] Gang Li *et al.*, arXiv:0807.1094.
[34] M. Altarawneh *et al.*, arXiv:0807.4488.

[35] A. Carrington, and F. Manzano, *Physica C* **385**, 205 (2003).
[36] H. G. Luo, and Tao Xiang, *Phys. Rev. Lett.* **94**, 027001 (2005).
[37] J. D. Fletcher *et al.*, *Phys. Rev. Lett.***98**, 057003 (2007).